



Co-function mechanism of multiple active sites over Ag/TiO₂ for formaldehyde oxidation

Xueyan Chen^{a,b}, Honghong Wang^{a,b}, Min Chen^{a,b}, Xiaoxiao Qin^{a,b}, Hong He^{a,b,c}, Changbin Zhang^{a,b,*}

^a State Key Joint Laboratory of Environment Simulation and Pollution Control, Research Center for Eco-Environmental Sciences, Chinese Academy of Sciences, Beijing 100085, China

^b University of Chinese Academy of Sciences, Beijing 100049, China

^c Center for Excellence in Regional Atmospheric Environment, Institute of Urban Environment, Chinese Academy of Sciences, Xiamen 361021, China

ARTICLE INFO

Keywords:

HCHO oxidation
Ag/TiO₂ catalysts
Inflection point
Co-function effect
Multiple active sites

ABSTRACT

Ag-based catalysts are shown to be efficient for formaldehyde (HCHO) oxidation at low temperature, while the role of active Ag species in this reaction remains a controversial issue. In this work, we prepared Ag/TiO₂ catalysts with TiO₂ of different crystal structures (anatase or rutile) as supports and tested their performances in HCHO oxidation. We observed that the crystal structure of the TiO₂ support had a significant influence on the activity of the Ag/TiO₂ catalysts, and Ag/A (anatase) exhibited dramatically superior activity compared with Ag/R (rutile). More interestingly, we observed a clear inflection point in the HCHO conversion curve for the Ag/R catalyst. Combining the results of BET, XRD, TEM, XAFS, H₂-TPR characterization and DFT calculations, we show that HCHO oxidation on Ag/TiO₂ catalysts is a co-function process of multiple active sites including surface oxygen, Ag₂O, and metallic Ag species. The low-temperature non-renewable surface oxygen and Ag₂O species mainly contribute to HCHO oxidation in the low-temperature range, while metallic Ag species are primarily responsible for the reaction at high temperature since metallic Ag is capable of activation of oxygen at high temperature. The relative contents of surface oxygen, Ag₂O and metallic Ag species are different on the Ag/A and Ag/R catalysts. The dispersion degree of metallic Ag species also differs on the Ag/A and Ag/R, therefore their capacities for oxygen activation are quite dissimilar. The above factors combine to result in distinct catalytic behaviors for Ag/A and Ag/R in HCHO oxidation, as well as the appearance of an inflection point.

1. Introduction

As one of the primary indoor air contaminants, formaldehyde (HCHO) has been known to cause adverse human health effects, such as eye irritation, respiratory illness, immune function impairment, and even cancer. [1–3] In view of its widespread use, toxicity and volatility, it is urgent to develop effective technologies for the elimination of indoor air HCHO. Various approaches, including adsorption [4], photocatalytic oxidation [5,6], plasma techniques [7,8], and thermal catalytic oxidation [9], have been investigated and applied for the removal of HCHO. Among them, thermocatalysis is a particularly promising technique because it can completely oxidize HCHO into harmless CO₂ and H₂O using suitable catalysts with high activity, stability, and reusability. [10,11]

Various types of catalysts have been developed for HCHO oxidation,

mainly classified as supported noble metal (Pt-, [12–17] Pd- [18–24], Rh- [25,26], Ir- [27], and Au- [28,29]) catalysts and transition-metal oxide (Co [10,30], Ce [31,32], Cu [33,34], Mn [34–38], etc.) catalysts. In general, the supported noble metal catalysts exhibit excellent activity for HCHO oxidation at ambient temperature, whereas their practical application is limited by the high prices and scarcity of the noble metal resources. In contrast, the transition-metal oxide catalysts are much cheaper and more plentiful, but their capacities for oxygen and water activation are relatively low at low temperature, therefore resulting in poor activity.

As one of the traditional precious metals, Ag has a much lower price than other precious metals, and has exhibited considerable efficiency for HCHO removal in the low temperature range. A recent study reported that 10 % Ag-8 % Mn/Beta-Si catalyst could achieve the full combustion of HCHO at 45 °C. [39] Therefore, Ag-based catalysts have

* Corresponding author at: State Key Joint Laboratory of Environment Simulation and Pollution Control, Research Center for Eco-Environmental Sciences, Chinese Academy of Sciences, Beijing 100085, China.

E-mail address: cbzhang@rcees.ac.cn (C. Zhang).

<https://doi.org/10.1016/j.apcatb.2020.119543>

Received 25 May 2020; Received in revised form 2 September 2020; Accepted 5 September 2020

Available online 22 September 2020

0926-3373/ © 2020 Elsevier B.V. All rights reserved.

attracted more attention in recent years, and the related study is one of the current hot topics [40–50]. Qu et al. [41] prepared a series of Ag-based catalysts on different supports and proposed that metallic Ag particles with subsurface oxygen in the bulk are more active for the adsorption and activation of HCHO than other active sites. In addition, they [42] also tested Ag/SBA-15 catalysts prepared by different methods, and found that high dispersion of Ag particles with a narrow size distribution contributes to their high catalytic activity for HCHO oxidation. Bai et al. [43,46] considered that Ag (111) crystal facets are active facets in Ag/Co₃O₄ and Ag/MnO₂ for the HCHO oxidation reaction. Huang et al. [50] reported that the partially oxidized state, Ag^{δ+} (0 < δ < 1), and high dispersion of Ag species are beneficial for the oxidation of HCHO over Ag/TiO₂ catalysts. Our previous studies [45,48] concluded that Ag species in the metallic state are favorable for oxygen activation during HCHO oxidation, and particle size and dispersion are also main factors affecting the catalytic performance. Apparently, researchers have different insights into the active sites and the structure-function relationship on Ag-based catalysts for the catalytic oxidation of HCHO.

In this study, we prepared 8 wt % Ag/TiO₂ catalysts with different TiO₂ crystal structure (anatase or rutile) supports by a co-impregnation method and investigated the roles of different Ag species on Ag/A and Ag/R in HCHO oxidation. Interestingly, we observed the appearance of an inflection point during the oxidation process. Based on the results of BET, XRD, TEM, XAFS, H₂-TPR characterization and DFT calculations, we propose that surface oxygen, Ag₂O, and metallic Ag species play their respective roles in HCHO oxidation, and the co-function effect of multiple active sites results in the different catalytic behaviors of the Ag/A and Ag/R catalysts and leads to the generation of an inflection point.

2. Experimental section

2.1. Materials preparation

The 8 wt % Ag/TiO₂ catalysts with different TiO₂ crystal structure (anatase or rutile) supports were prepared by co-impregnation of anatase (Alfa) or rutile (Aladdin) with aqueous AgNO₃. After stirring for 1 h, the excess water was removed in a rotary evaporator at 55 °C. Then, the samples were dried at 100 °C for 4 h and calcined at 450 °C for 3 h afterwards. The as-prepared samples were denoted as Ag/A and Ag/R, respectively. After the fresh Ag/A and Ag/R were tested, the tested samples were designated as the Ag/A-spent, Ag/R-spent. The Ag/TiO₂-spent catalysts were next treated in a flow of air (20 % O₂) at temperatures of 100 °C, 140 °C and 300 °C, and the treated samples were named as the Ag/A-spent-100, Ag/A-spent-140, Ag/A-spent-300 and the Ag/R-spent-100, Ag/R-spent-140, Ag/R-spent-300.

2.2. Material characterization

XRD, N₂ adsorption – desorption analysis, TEM, and XAFS experiments were carried out according to our previous work [48].

H₂ temperature-programmed reduction (H₂-TPR) was performed in a Micromeritics AutoChem II 2920 apparatus, equipped with a computer-controlled CryoCooler and a thermal conductivity detector (TCD). The reduction profiles were obtained by passing a flow of 10 % H₂/Ar at a rate of 50 mL min⁻¹ (STP) through the sample (weight around 50 mg). The temperature was increased from 30 to 350 °C at a rate of 10 °C min⁻¹.

2.3. DFT calculation methods

Geometry optimization and energy calculations were carried out using the Vienna Ab-initio Simulation Package (VASP 5.4.1) [51]. The projected augmented-wave (PAW) [52,53] method was employed to describe the interactions between ions and electrons. The wave

functions and exchange-correlation function were elucidated by a plane wave basis set and PBE generalized gradient approximation [54], respectively. The cutoff energy for the plane-waves was set to 400 eV. The Brillouin zone was sampled using 3 × 3 × 1 and 3 × 2 × 1 k point Monkhorst–Pack grids for anatase (101) and rutile (110), respectively, during the surface and adsorption geometry optimization. The Gaussian smearing method with a smearing width of 0.2 eV was employed to accelerate the convergence of integration at the Brillouin zone. A 1 × 3 supercell with three TiO₂ layers was built for the anatase (101) surface, and a 3 × 2 supercell with three TiO₂ layers was built for the rutile (110) surface. A vacuum layer of 15 Å between adjacent slabs was included to reduce the interaction energy between slabs. In the computation, the bottom two layers of the slab were fixed and the top three layers and Ag₅ cluster were fully relaxed until the forces on each atom were less than 0.02 eV/Å. The static calculation of the O₂ decomposition reaction on two catalyst surfaces was carried out at 273 K. The minimum energy path of the O₂ dissociation reaction pathway was calculated via the climbing image nudged elastic band (CI-NEB) method with a 0.05 eV Å⁻¹ force converged threshold.

The adsorption energies (E_{ads}) of the Ag₅ cluster on the surface were calculated as:

$$E_{\text{ads}} = E_{\text{slab-x}} - (E_{\text{slab}} + E_x)$$

where E_{slab}, E_x and E_{slab-x} refer to the energy of the anatase (101) surface or rutile (110) surface model, Ag₅ in the gaseous phase, and the anatase-Ag₅/rutile-Ag₅ supersystem. According to the above equation, negative values of E_{ads} indicate an exothermic reaction and positive values indicate that adsorption does not occur.

2.4. Activity test for HCHO oxidation

The activity tests for the catalytic oxidation of HCHO over the catalysts (60 mg) were performed in a fixed-bed quartz flow reactor with feed gas composed of 130 ppm of HCHO, 20 % O₂, with or without 35 % relative humidity (RH), and helium balance; the total flow rate was 100 mL min⁻¹, corresponding to a weight hourly space velocity (WHSV) of 100, 000 mL/(g_{cat} h). Gaseous HCHO was obtained by flowing helium through a paraformaldehyde container in a water bath, and the concentration of inlet HCHO was controlled by adjusting the temperature of the water bath. [48] Similarly, Water vapor was generated by flowing helium through a water bubbler at 25 °C, and the relative humidity in the reaction atmosphere was controlled by adjusting the flow rate of the purging helium and measured by a hygrometer. For the Ag/A catalyst, the residence time for each temperature point was 1 h, except for 35 °C, for which the time was 1.5 h. The hold time at each temperature was 1.5 h for 35, 95, 110, 125, 140, 155 °C and 1 h for 65, 170, 185, 215, 245 °C for the Ag/R catalyst. Analysis of inlet and outlet gases and the carbon balance calculation were performed according to our previous study [12]. For cycling testing, both Ag/A and Ag/R catalysts were tested 5 times in the absence of water vapor. The first and second tests were for fresh and spent catalysts, respectively, and the spent catalysts were re-oxygenated before the subsequent three tests with processing temperatures of 100 °C, 140 °C, and 300 °C.

3. Results

3.1. Activity test

The performances of the Ag/A and Ag/R catalysts together with pure anatase and rutile supports for HCHO oxidation are presented in Fig. 1 and Fig S1. As shown in Fig S1, both of pure anatase and rutile supports showed rather poor activities in the test temperature range. Whereas, the crystal structure of the TiO₂ support had a remarkable influence on the activity of the Ag/TiO₂ catalysts, and the Ag/A catalyst exhibited much superior activity compared to the Ag/R catalyst (shown

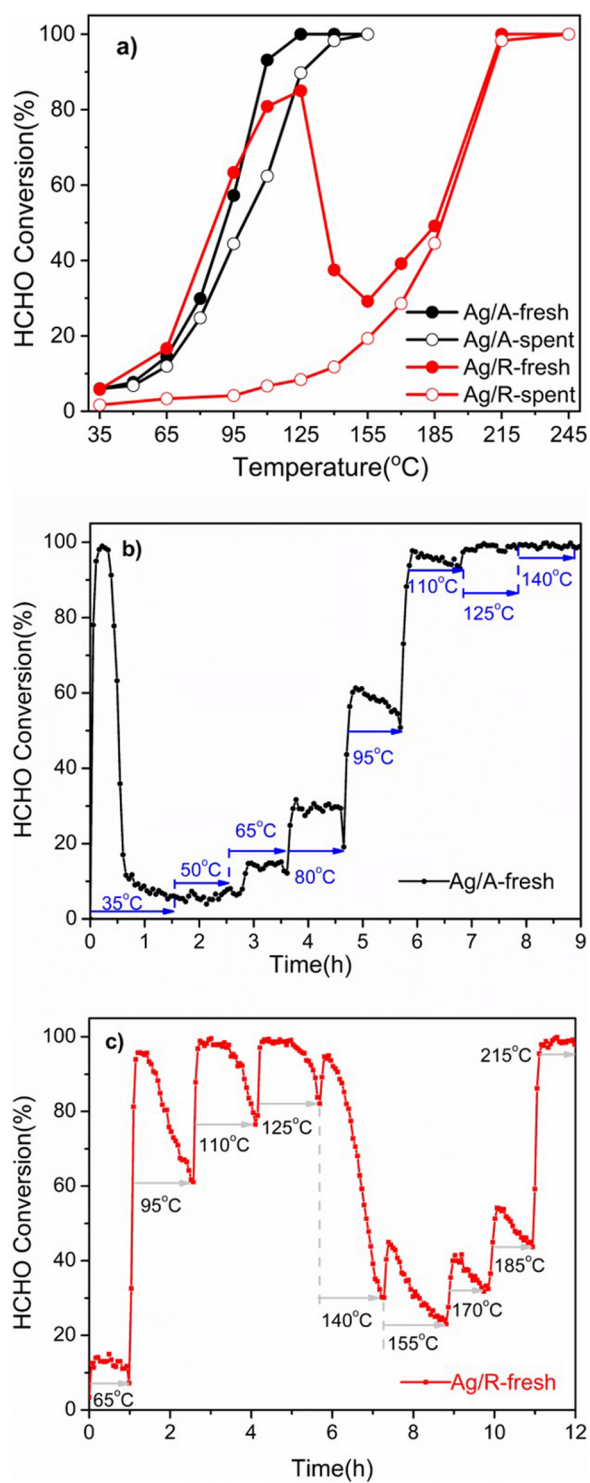


Fig. 1. a) HCHO conversion over fresh and spent Ag/A and Ag/R catalysts, and the change tendency of HCHO conversion with temperature and time-on-stream on b) Ag/A-fresh catalyst, and c) Ag/R-fresh catalyst. Reaction conditions: 130 ppm of HCHO, 20 % O₂, He balance, WHSV 100 000 mL/(g_{cat} h).

in Fig. 1a). Complete HCHO conversion (100 %) was reached at 125 °C for the fresh Ag/A catalyst at the space velocity of WHSV = 100,000 mL/(g_{cat} h). In contrast, HCHO could not be completely removed until 215 °C on the fresh Ag/R catalyst under the same conditions. Interestingly, we also observed an inflection point in the curve of HCHO conversion on the fresh Ag/R catalyst. In the range of 35 °C–125 °C, the HCHO conversion on the Ag/R catalyst gradually

increased with temperature, and 85 % of HCHO could be removed at 125 °C. Subsequently, when the temperature rose from 125 °C to 155 °C, the HCHO removal efficiency sharply decreased and dropped to only 29 % at 155 °C. Afterwards, the HCHO conversion was improved once again with the further increment of temperature above 155 °C, until 130 ppm of HCHO was completely eliminated at around 215 °C.

We also analyzed the change tendency of HCHO conversion with temperature and time-on-stream. As shown in Fig. 1b and c, at certain temperatures, the HCHO conversion on both the Ag/A-fresh and Ag/R-fresh catalysts continuously changed with time-on-stream and could not reach a steady state. In particular, Ag/R-fresh demonstrated drastic changes in HCHO conversion during the test periods, and a sharp drop in HCHO conversion with time was clearly observed at around 150 °C. The decreasing tendency of HCHO conversions on Ag/TiO₂-fresh may be due to the accumulation of intermediate species [50] or the changes of active species on catalyst surface. Dioxymethylene (DOM) and HCOO species are two key intermediates in HCHO oxidation, and these two species are mainly adsorbed on the TiO₂ surface [15,27,55–57]. It is shown that the formation and transformation of intermediate species greatly depend on the content and reactivity of active species. Hence, the changes of active species should be the essential reason for the activity fluctuations and the appearance of inflection point on Ag/TiO₂ catalysts. We subsequently conducted a second testing of the spent Ag/A and Ag/R catalysts. As shown in Fig. 1a, the Ag/A-spent showed a slight decrease in activity compared with the fresh Ag/A catalyst, but still reached 90 % HCHO conversion at 125 °C. In contrast, the Ag/R-spent catalyst almost completely lost its activity for HCHO oxidation at temperatures below 125 °C and the inflection point also disappeared; however, it had very similar activity to the fresh Ag/R catalyst at higher temperature (> 150 °C).

We next treated the spent Ag/A and Ag/R catalysts in a flow of air (20 % O₂) at temperatures of 100 °C, 140 °C and 300 °C, respectively. The treated catalysts were next tested for HCHO oxidation, and the test results are shown in Fig. 2. The O₂ treatment at 100 °C had no influence on Ag/A-spent, and the activity of Ag/A-spent-100 was almost the same as that of Ag/A-spent (Fig. 2a). When the treatment temperature was increased to 140 °C, the activity of Ag/A-spent-140 was clearly improved, and was close to that of fresh Ag/A catalyst. After the treatment at 300 °C, the activity of Ag/A-spent-300 was completely recovered back to that of the fresh Ag/A catalyst. As shown in Fig. 2b, after oxygen treatment at 100 °C, the Ag/R-spent-100 catalyst still remained inactive at low-temperature range and no inflection point appeared. The treatment at 140 °C significantly increased the HCHO removal performance of the Ag/R-spent-140 catalyst and the inflection point also appeared again. The treatment at 300 °C also totally re-activated the Ag/R-spent to the level of the fresh Ag/R catalyst.

These results above indicate that the active sites or active species responsible for HCHO oxidation may be different in the low and high temperature ranges on Ag/TiO₂ catalysts (especially for Ag/R). The activity test for fresh samples consumes the active oxygen species responsible for HCHO oxidation in the low-temperature range, therefore resulting in a decrease in the activity of the spent sample and the disappearance of the inflection point. However, the testing had no obvious influence on the active oxygen species contributing to HCHO oxidation at high temperature. The O₂ treatment at high temperature (300 °C) could restore the active oxygen species for low-temperature HCHO oxidation, therefore reproducing their catalytic behavior.

We also tested the Ag/A and Ag/R catalysts in the presence of water vapor. As shown in Fig S2, two catalysts both behaved differently in RH 35 % than in dry reaction atmosphere. The activity of Ag/A was severely suppressed by water vapor in the entire temperature range. The performance of Ag/R fluctuated in the low-temperature range, while it remained almost unchanged at high temperature. Notably, an inflection point still clearly appeared on Ag/R catalyst. Water vapor can compete with HCHO for adsorption on surface, and also it can be activated by Ag to form surface OH groups participating in HCHO oxidation [43,48]

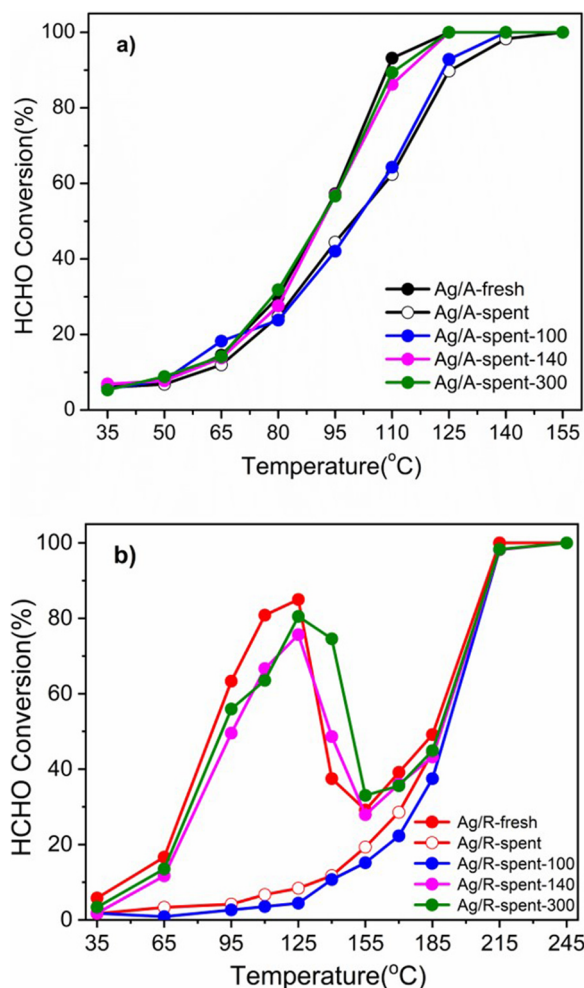


Fig. 2. HCHO conversion over O_2 -treated Ag/TiO₂-spent catalysts a) Ag/A, and b) Ag/R. Reaction conditions: 130 ppm of HCHO, 20 % O_2 , He balance, WHSV 100 000 mL/(g_{cat} h).

Hence, the changes in activities of Ag/A and Ag/R should be due to the dual function of water vapor. In view of the complexity of water influence on activity, we here mainly focus on the performances of the catalysts in the absence of water vapor, and discuss the influence of oxygen species on activity separately.

3.2. Structural features and chemical states of catalysts

In order to explain the reasons for the different catalytic behaviors of the Ag/A and Ag/R catalysts, and also the appearance of an inflection point during the testing of Ag/R, the catalysts were next carefully characterized. BET measurements were conducted to examine the physical properties of the samples. The specific surface areas, pore sizes and pore volumes of the anatase, Ag/A, rutile and Ag/R samples are summarized in Table 1. The specific surface areas of the pure anatase and rutile supports were 86.1 m²/g and 26.9 m²/g, respectively. After 8 % Ag was loaded, the surface areas of Ag/A and Ag/R samples

Table 1
Physical Parameters of anatase, Ag/A, rutile and Ag/R samples.

Samples	S _{BET} (m ² /g)	Pore volume (ml/g)	Pore diameter (nm)
Anatase	86.1	0.48	20.0
Ag/A	35.3	0.30	27.4
Rutile	26.9	0.14	25.4
Ag/R	20.0	0.12	26.8

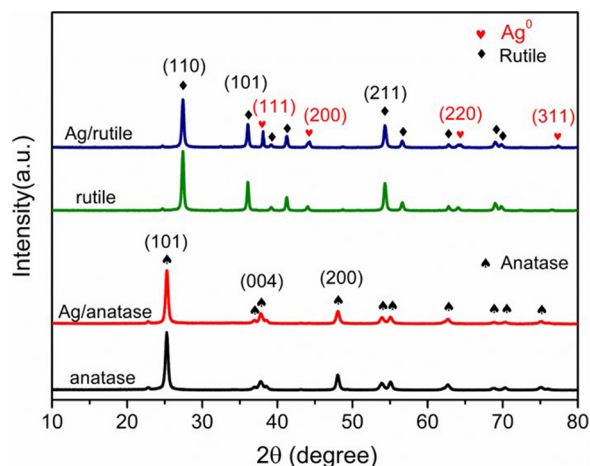


Fig. 3. XRD patterns of anatase, Ag/A, rutile and Ag/R samples.

decreased to 35.3 m²/g and 20.0 m²/g. The specific surface area of Ag/A was about 1.5 times higher than that of the Ag/R catalyst, and the larger specific surface area of Ag/A should be more favorable for the dispersion of Ag species and the adsorption of HCHO.

XRD measurements were carried out to investigate the crystal structures of the samples, and the results of TiO₂ supports and fresh samples are shown in Fig. 3. The intense peaks at the characteristic angles of TiO₂ for the anatase (JCPDS 21–1272) and rutile (JCPDS 21–1276) structures indicated the dominant contents of the respective supports. The XRD pattern of the Ag/A catalyst only exhibited the diffraction peaks of the anatase support and no Ag species (Ag⁰, Ag₂O) were observed, indicating that Ag species were well dispersed on anatase. In contrast, after Ag was loaded on the rutile support, the (111), (200), (220) and (311) reflections of crystalline metallic Ag (JCPDS 65–2871), corresponding to 38.1°, 44.3°, 64.4° and 77.5° (2θ), [41,45,58] were observed, indicating that the crystallinity of metallic Ag species on rutile was much higher than that on anatase. Thus, we speculated that Ag with much larger particle size or greater amounts of metallic Ag species existed on Ag/R compared with the Ag/A catalyst. The XRD patterns of the spent catalysts were also characterized and shown in Fig S3. After activity tests, the diffraction peaks of Ag⁰ species appeared on Ag/A-spent catalyst, demonstrating the agglomeration of Ag⁰ particles and the reduction of Ag₂O species on the fresh Ag/A during HCHO oxidation process. In contrast, the crystallinity of metallic Ag on the Ag/R-spent did not change obviously, indicating that the particle sizes of Ag species were basically the same as the fresh one.

We next implemented TEM and XAFS measurements to investigate the particle size distribution and chemical states of Ag species on the Ag/A and Ag/R catalysts. Fig. 4 and Fig S4 present the TEM images of the fresh and spent Ag/A and Ag/R samples and the inset histograms are the statistical results from 350 particles. As shown in Fig. 4a, Ag species on the Ag/A catalyst mainly existed in the form of small particles and showed good dispersion. From the results of particle size statistics, the sizes of Ag particles on Ag/A were primarily below 4 nm, with an average diameter of 2.9 nm. After activity test, the average diameter of Ag particles increased up to 3.8 nm on the Ag/A-spent catalyst (Fig S4a). For the Ag/R catalyst (Fig. 4b), significant agglomeration of Ag species could be observed. The Ag particles displayed a wider distribution on the Ag/R catalyst, and the average particle size of Ag species reached 4.5 nm. HCHO oxidation process did not significantly affect the average particle size of Ag species on the Ag/R catalyst (Fig S4b). The TEM results are consistent with the results of BET and XRD.

Fig. 5 shows the Ag – K XANES of Ag/A and Ag/R catalysts, AgNO₃, and Ag foil. According to the positions of the white line, we can clearly see that the Ag – K absorption edges of both Ag/A and Ag/R samples

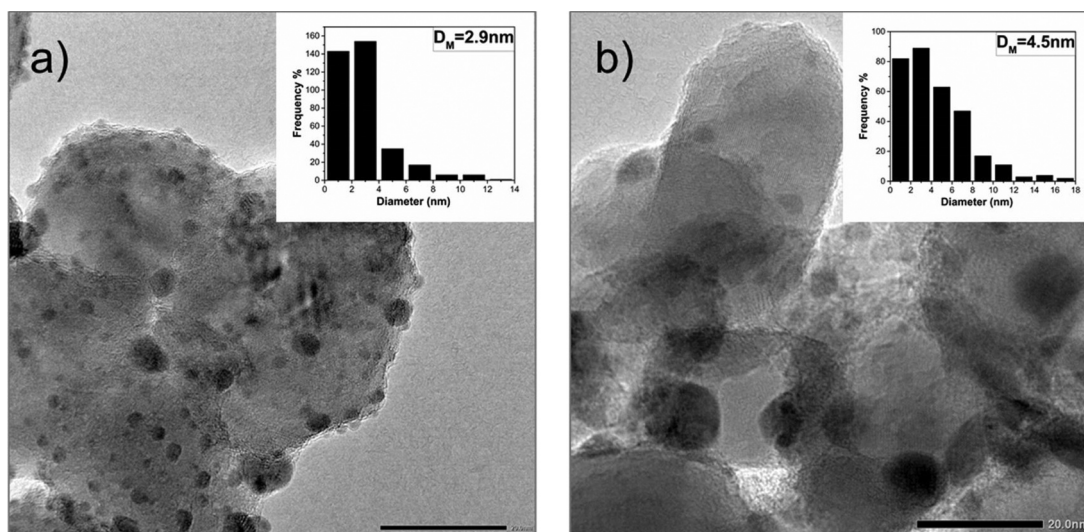


Fig. 4. TEM images and the average Ag particle size distributions of Ag/A (a) and Ag/R (b) catalysts.

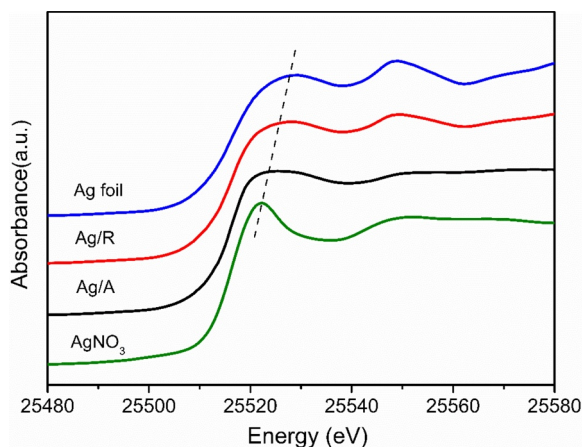


Fig. 5. Normalized Ag – K XANES for Ag/A and Ag/R catalysts.

Table 2
LC-XANES fits of Ag-K in Ag/A and Ag/R catalysts.

Samples	Ag ⁰ (%)	Ag ⁺ (%)
Ag/A	15.3	84.7
Ag/R	61.9	38.1

were located between those of Ag foil and AgNO₃, indicating that Ag species on both the Ag/A and Ag/R samples existed in a mixed state with partial metallic and partial oxidized state. In addition, the absorption edge of Ag/A was closer to that of AgNO₃, while that of Ag/R was nearer to Ag foil. We further performed (linear combination) LC-XANES fits for the samples to determine the contents of Ag species with different valences. Based on a principal component analysis, we chose Ag foil, Ag₂O and AgNO₃ as model compounds. The fitting results are summarized in Table 2, and the fitted figures are shown in Fig S5. The proportions of metallic Ag in Ag/A and Ag/R samples were 15.3 % and 61.9 %, respectively, demonstrating that the Ag species were mainly in the oxidized state on Ag/A catalyst, while metallic Ag was dominant on the Ag/R sample.

3.3. Reducibility of catalysts

H₂-TPR experiments were next conducted to investigate the reducibility of the catalysts, and the TPR profiles of the fresh and spent

(after HCHO activity test) Ag/A and Ag/R catalysts are shown in Fig. 6a. The overlapped H₂ reduction peaks on the fresh Ag/A catalyst were deconvoluted into several sub-bands by searching for the optimal combination of Gaussian bands with correlation coefficients (r^2) above 0.99 and without fixing the sub-band positions (PeakFit software package, Version 4.12, SeaSolve Software Inc.). The profiles of the fresh Ag/A sample showed three reduction peaks at 63, 112 and 256 °C, which were ascribed to the reduction of oxygen species adsorbed on the surface on dispersed metallic Ag, large Ag₂O clusters, and small Ag₂O clusters, respectively, [45,59] revealing the co-existence of diverse Ag species on the fresh Ag/A catalyst. Nevertheless, only one H₂ consumption peak at 63 °C was clearly observed on the fresh Ag/R catalyst, and this peak was also due to the reduction of surface oxygen adsorbed on metallic Ag. The absence of H₂ consumption peaks corresponding to Ag₂O species on Ag/R demonstrates that the amount of Ag oxides on Ag/R is much lower than that on Ag/A, which is consistent with the LC-XANES fitting results. The H₂ consumption amount related to the peaks at 63 °C on Ag/A and Ag/R catalysts were next calculated and presented in Table 3. Clearly, the H₂ consumption amount for Ag/A (56.1 μmol/g) was significantly higher than that for Ag/R (26.1 μmol/g), indicating that there were more surface oxygen species on Ag/A. Combined with the XANES and LC-XANES fitting results, Ag/A had less metallic Ag but more surface chemisorbed oxygen than Ag/R, which might be ascribed to the synergistic effect of the number of Ag sites, Ag particle size, and the capacity of metallic Ag for oxygen activation. The BET, XRD and TEM results show that the anatase support had a larger specific surface area than rutile, which is favorable for the dispersion of Ag species, thus resulting in more Ag sites with smaller particle sizes. As with the literatures on the catalysis of Ag species, the small-sized Ag particles have the stronger oxygen activation ability. [60] In addition, considering the differences in interaction between Ag and the different supports, the capacities of Ag particles with the same size for oxygen activation might also be different on the anatase and rutile supports.

As for both Ag/A-spent and Ag/R-spent catalysts, no H₂ consumption peaks for surface oxygen appeared, indicating that the surface oxygen species on metallic Ag were depleted in the HCHO oxidation reaction and could not be regenerated during cooling down to room temperature in a flow of O₂ + HCHO + He after testing. In contrast, two H₂ consumption peaks corresponding to large and small Ag₂O clusters were still observed on the Ag/A-spent catalyst, but these two peaks moved to higher temperatures, from 112, 256 °C to 139, 283 °C, respectively. We therefore believe that Ag₂O species participated in the oxidation reaction of HCHO. The Ag₂O species on the fresh sample were reduced during the reaction and coalesced into metallic Ag species, and

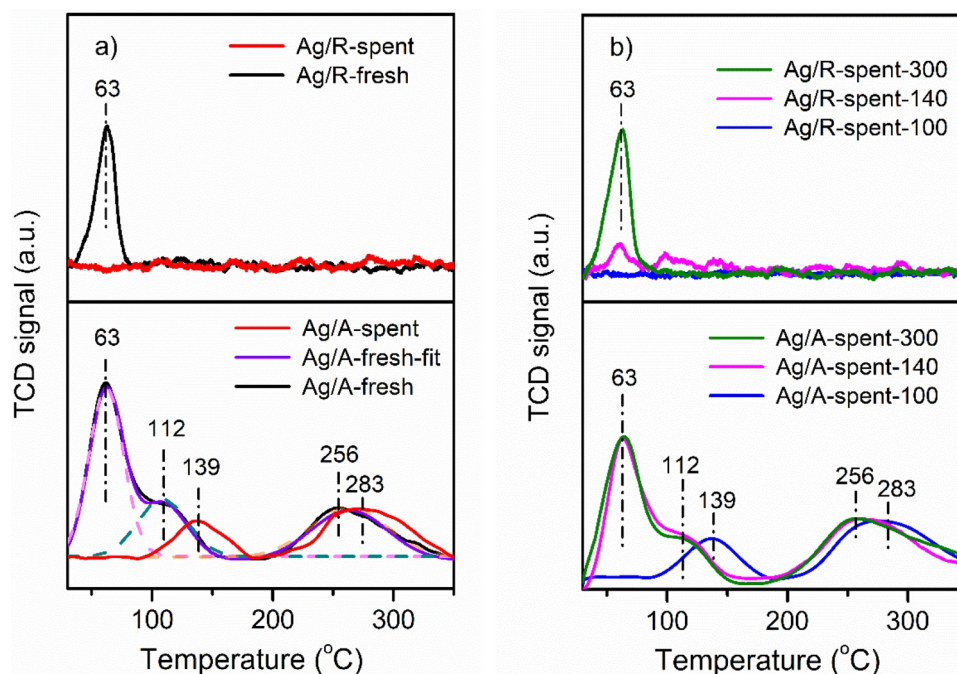


Fig. 6. H₂-TPR profiles of a) fresh and spent Ag/A and Ag/R catalysts, and b) Ag/A-spent and Ag/R-spent catalysts treated with 20 % O₂ at different temperatures.

Table 3

H₂ consumption of Ag/A and Ag/R catalysts in H₂-TPR at 63 °C.

Samples	H ₂ consumption in H ₂ -TPR at 63 °C (μmol/g)
Ag/A	56.1
Ag/R	26.1

these metallic Ag species could be partially oxidized during the cooling process, re-forming Ag₂O species with smaller particle size on the Ag/A-spent catalyst.

The spent Ag/A and Ag/R catalysts were treated with 20 % O₂ at 100 °C, 140 °C, and 300 °C, and H₂-TPR experiments were next carried out on the treated samples. As shown in Fig. 6b, the O₂ treatment at 100 °C had no obvious influence on the reducibility of the Ag/A-spent and Ag/R-spent catalysts, and their H₂ consumption profiles were similar to those before treatment, indicating that metallic Ag on Ag/A and Ag/R catalysts still could not activate oxygen at 100 °C. When the treatment temperature was increased to 140 °C, the peak for surface oxygen species was almost recovered on the Ag/A-spent catalyst, but was still very weak on the Ag/R-spent sample, demonstrating that the metallic Ag on Ag/A had better capacity for oxygen activation at 140 °C than the metallic Ag on Ag/R. Besides, the reduction peaks for Ag₂O particles on the Ag/A catalyst shifted back to their original temperatures, indicating that the Ag₂O species were restored to its initial state. After the 300 °C oxygen treatment, both Ag/A-spent and Ag/R-spent catalysts exhibited the same TPR profiles as their fresh counterparts, revealing that both surface oxygen species and Ag₂O species were totally recovered.

Combined with the activity test results, it is clear that surface oxygen, metallic Ag and Ag₂O species all play their respective roles in HCHO oxidation. Specifically, the non-renewable surface chemisorbed oxygen and Ag₂O species contribute to HCHO oxidation at low temperature, and the metallic Ag species are responsible for the reaction at high temperature. For the fresh Ag/A catalyst, there are more chemisorbed oxygen and Ag₂O species on the surface, thereby providing high catalytic performance and also guaranteeing the smooth progress of HCHO oxidation in the low-temperature range. When the reaction temperature reaches 140 °C, the metallic Ag can effectively activate

oxygen species, thus ensuring the continuity of the reaction. In contrast, there is only a relatively small amount of low-temperature non-renewable surface oxygen and Ag₂O species on the Ag/R catalyst. After the surface oxygen species are quickly consumed and the Ag₂O species are completely reduced, HCHO oxidation depends only on the activation of the oxygen on metallic Ag species. When the metallic Ag species on the Ag/R catalyst cannot activate oxygen at certain temperatures, the HCHO conversion will decrease until the metallic Ag has sufficient capacity to activate oxygen, therefore resulting in the appearance of an inflection.

For the spent Ag/TiO₂ catalysts, the surface oxygen species were depleted, and the oxygen supply capacity of Ag₂O species became worse due to the reduction of Ag₂O species, thus resulting in the drop of low-temperature activities. Besides, the high-temperature activity of Ag/A-spent catalyst also showed a slight decrease because of the increase of metallic Ag particles size. The average Ag particle size on Ag/R-spent catalyst did not change apparently and the high-temperature activity of Ag/R-spent remained. With 20 % O₂ treatment at 140 °C, the HCHO oxidation performance of Ag/A-spent-140 catalyst was close to that of the fresh one since the surface oxygen, Ag₂O and the ability of Ag⁰ to activate oxygen were almost totally recovered. The low-temperature activity of the Ag/R-spent-140 catalyst was also distinctly improved on account of the partial recovery of surface oxygen and Ag₂O. When the O₂ treatment temperature rose to 300 °C, the surface oxygen and Ag₂O species on both Ag/A-spent and Ag/R-spent catalysts are restored, and their performances for HCHO oxidation is comparable to that of the fresh Ag/A and Ag/R catalysts, showing the excellent recyclability of the two catalysts.

3.4. DFT calculations

DFT calculations were next conducted to investigate the adsorption and activation of O₂ on the metallic Ag species on the Ag/A and Ag/R catalysts. According to the TEM images, the average particle sizes of Ag species on Ag/A and Ag/R were 2.9 nm and 4.5 nm, respectively. These nanoscale Ag particles, as reported in the literature, [61] contain thousands of Ag atoms. Besides, the size distribution of Ag particles was also much different between Ag/A and Ag/R catalysts. Hence, the computational model was simplified, and Ag₅/A and Ag₅/R models

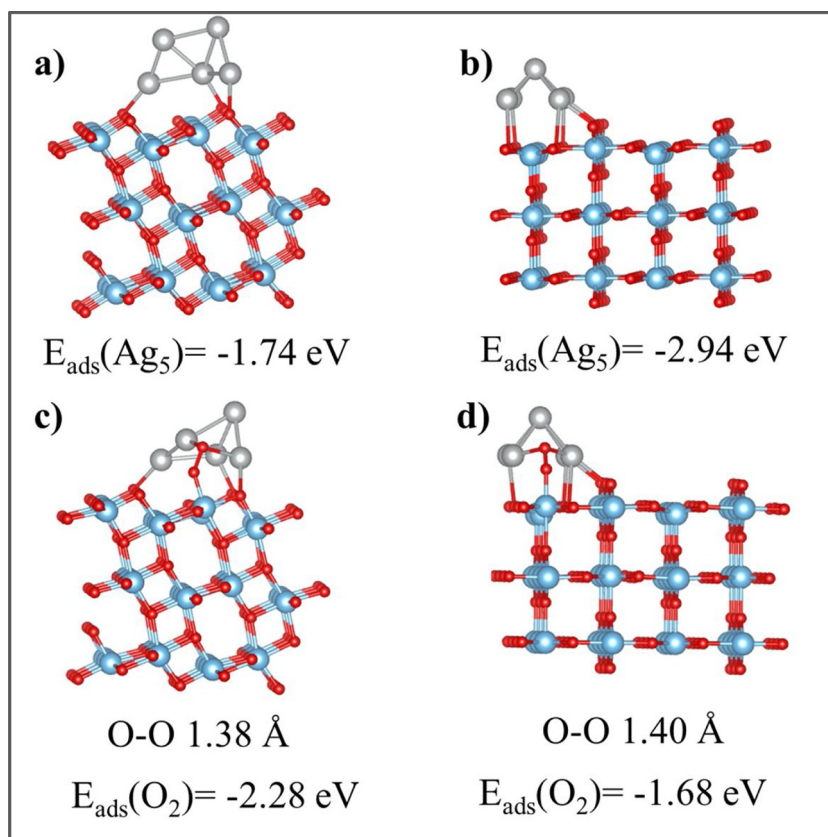


Fig. 7. Optimized stable structures of Ag_5 cluster adsorption on a) anatase and b) rutile surface, and O_2 adsorption on c) Ag_5/A and d) Ag_5/R interface.

were selected for calculations. Specifically, we optimized two Ag_5 clusters (in planar and nonplanar form, C_{2v}) in the gas phase and then adsorbed them on the stoichiometric anatase (101) and rutile (110) surfaces, and their optimized stable structures are illustrated in Fig. 7a and b. The Ag_5 cluster configurations were different in the Ag_5/A and Ag_5/R systems. The adsorption energy of Ag_5 clusters on anatase and rutile was -1.74 eV and -2.94 eV , respectively, indicating that the Ag_5 cluster bonded more strongly on rutile (110) than on the anatase (101) surface. Then, the corresponding stable binding structures and adsorption energies of O_2 on Ag_5/A and Ag_5/R were calculated and displayed in Fig. 7c and 7d. The five-coordinated surface Ti atoms (Ti_{5c}) participated in the adsorption of O_2 , and the two interfacial Ag sites near the surface Ti_{5c} atoms would be also the adsorption sites for anchoring O_2 . That is, one oxygen atom in O_2 was bonded to a surface Ti_{5c} atom while the other oxygen atom was linked to two Ag atoms. The interaction between O_2 and Ag_5/A (101) was stronger than that between O_2 and Ag_5/R (110). Fig. 8 shows the dissociation processes of O_2 on the optimized Ag_5/A and Ag_5/R surfaces. We could see that O_2 dissociation processes at the interfacial sites were thermodynamically favorable, evidenced by their exothermic characteristics (more than 0.86 eV). Moreover, since the energy barrier for the dissociation process on the Ag_5/A (101) interface ($E_a = 0.29 \text{ eV}$) was much lower than that on the Ag_5/R (110) interface ($E_a = 0.52 \text{ eV}$), the O_2 activation at Ag_5/A (101) would be kinetically preferable compared to that of Ag_5/R (110), suggesting that Ag_5/A (101) has a higher capacity for oxygen activation than Ag_5/R (110). These results are fully consistent with the testing performance and H_2 -TPR results.

4. Discussion

The activity test results show that the crystal structure of the TiO_2 support has a remarkable influence on the activity of the Ag/TiO_2 catalysts for HCHO oxidation. The Ag/A catalyst demonstrates much

superior performance compared with the Ag/R catalyst. Additionally, fluctuations in HCHO conversion profiles are observed at certain temperatures on both of Ag/A and Ag/R catalysts, and an especially clear inflection point appears for the Ag/R catalyst. The different catalytic behaviors of Ag/A and Ag/R catalysts are closely related to the valence state, relative contents in different valence states and dispersion of Ag species.

The XAFS results and H_2 -TPR profiles of fresh Ag/TiO_2 catalysts show that there are less metallic Ag species, but more amounts of Ag_2O species and more chemisorbed oxygen on the surface of the Ag/A catalyst compared with those on the Ag/R catalyst. The TPR results of Ag/TiO_2 -spent and Ag/TiO_2 -spent-100 catalysts clearly show that the surface oxygen and Ag_2O species participate in HCHO oxidation in the low-temperature range, since the metallic Ag was not capable of O_2 activation at low temperature, indicating that the superior catalytic performance of the Ag/A catalyst at low temperature should be due to the abundant non-renewable surface oxygen and Ag_2O species on the Ag/A surface.

The BET, XRD and TEM results show that the Ag/A catalyst has a larger specific surface area than the Ag/R catalyst, and therefore is more favorable for the dispersion of Ag species. The Ag/A catalyst contains more active Ag sites with smaller particle sizes and a narrower particle size distribution compared with the Ag/R catalyst. The high dispersion and narrow distribution of Ag particle size on Ag/A is greatly beneficial for HCHO oxidation. [42] Apart from this, DFT calculations further confirm that metallic Ag species with the same particle size have a stronger oxygen activation capacity on anatase than on rutile. The large number of metallic Ag sites on Ag/A and the high ability of metallic Ag to activate oxygen lead to the superior performance of the Ag/A catalyst for HCHO oxidation in the middle- and high-temperature ranges. In contrast, the small number of metallic Ag sites on Ag/R and its low ability to activate oxygen result in its poor performance for HCHO conversion compared with Ag/A .

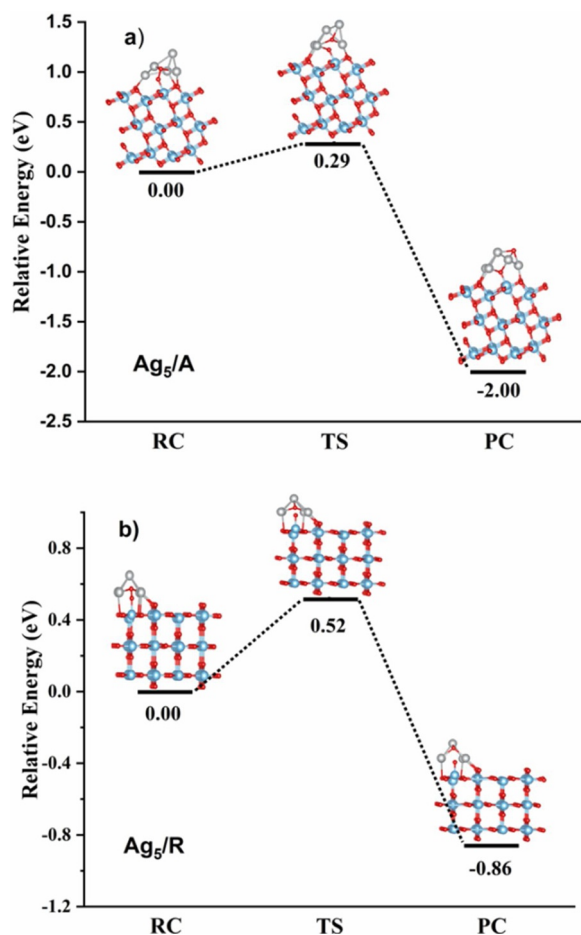


Fig. 8. Potential energy surfaces of O₂ dissociation on a) Ag₅/A and b) Ag₅/R surface.

Based on the above analysis, we believe that the HCHO oxidation reaction on Ag/TiO₂ catalysts is a co-function process involving multiple active sites. The non-renewable surface oxygen and Ag₂O species are the main active species for HCHO oxidation at low temperature, while the metallic Ag species are the main active sites at high temperature. The abundant surface oxygen and Ag₂O species coupled with the high capacity of metallic Ag species for oxygen activation contribute to the excellent activity of the Ag/A catalyst for HCHO oxidation. The small amount of chemisorbed surface oxygen and Ag₂O species as well as insufficient oxygen activation ability of metallic Ag on the Ag/R catalyst induce a supply dilemma for active oxygen species during the period of surface oxygen depletion, and eventually leading to a sharp drop in HCHO conversion and the appearance of an inflection point in the middle temperature range.

5. Conclusions

In summary, this work demonstrates that the crystal structure of the TiO₂ support has a great influence on the activity of Ag/TiO₂ catalysts for HCHO oxidation, and the Ag/A catalyst exhibits much superior activity compared to the Ag/R catalyst. We reveal that HCHO oxidation on Ag/TiO₂ catalysts is a co-function process involving multiple active sites, and surface chemisorbed oxygen, Ag₂O, and metallic Ag species all play important roles in the reaction: non-renewable surface oxygen and Ag₂O species account for the supply of active oxygen species for HCHO conversion in the low-temperature regime, while metallic Ag species are responsible for the activation of oxygen in the high-temperature range. The differences in relative contents and capacities of active species for oxygen activation lead to the different catalytic

behaviors of the Ag/A and Ag/R catalysts in HCHO oxidation, especially the occurrence of the inflection point on Ag/R.

CRediT authorship contribution statement

Xueyan Chen: Conceptualization, Methodology, Data curation, Investigation, Formal analysis, Writing - original draft, Writing - review & editing. **Honghong Wang:** Validation, Investigation, Software, Formal analysis, Writing - review & editing. **Min Chen:** Validation, Investigation, Formal analysis. **Xiaoxiao Qin:** Validation, Investigation, Formal analysis. **Hong He:** Investigation, Resources, Supervision. **Changbin Zhang:** Conceptualization, Methodology, Investigation, Validation, Formal analysis, Project administration, Resources, Writing - review & editing, Supervision.

Declaration of Competing Interest

The authors reported no declarations of interest.

Acknowledgments

This work was financially supported by the National Key R&D Program of China (2017YFC0211802) and National Natural Science Foundation of China (21976196, 21906174).

Appendix A. Supplementary data

Supplementary material related to this article can be found, in the online version, at doi:<https://doi.org/10.1016/j.apcatb.2020.119543>.

References

- [1] L. Nie, J. Yu, M. Jaroniec, F.F. Tao, Room-temperature catalytic oxidation of formaldehyde on catalysts, *Catal. Sci. Technol.* 6 (2016) 3649–3669, <https://doi.org/10.1039/c6cy00062b>.
- [2] T. Salthammer, S. Mentese, R. Marutzky, Formaldehyde in the indoor environment, *Chem. Rev.* 110 (2010) 2536–2572, <https://doi.org/10.1021/cr800399g>.
- [3] B. Bai, Q. Qiao, J. Li, J. Hao, Progress in research on catalysts for catalytic oxidation of formaldehyde, *Chinese J. Catal.* 37 (2016) 102–122, [https://doi.org/10.1016/S1872-2067\(15\)61007-5](https://doi.org/10.1016/S1872-2067(15)61007-5).
- [4] C. Ma, X. Li, T. Zhu, Removal of low-concentration formaldehyde in air by adsorption on activated carbon modified by hexamethylene diamine, *Carbon* 49 (2011) 2873–2875, <https://doi.org/10.1016/j.carbon.2011.02.058>.
- [5] T. Noguchi, A. Fujishima, P. Sawunyama, K. Hashimoto, Photocatalytic degradation of gaseous formaldehyde using TiO₂ film, *Environ. Sci. Technol.* 32 (1998) 3831–3833, <https://doi.org/10.1021/es980299+>.
- [6] X. Zhu, C. Jin, X.-S. Li, J.L. Liu, Z.G. Sun, C. Shi, X. Li, A.M. Zhu, Photocatalytic formaldehyde oxidation over plasmonic Au/TiO₂ under visible light: moisture indispensability and light enhancement, *ACS Catal.* 7 (2017) 6514–6524, <https://doi.org/10.1021/acscatal.7b01658>.
- [7] M.B. Chang, C.C. Lee, Destruction of formaldehyde with dielectric barrier discharge plasmas, *Environ. Sci. Technol.* 29 (1995) 181–186, <https://doi.org/10.1021/es00001a023>.
- [8] X. Zhu, X. Gao, R. Qin, Y. Zeng, R. Qu, C. Zheng, X. Tu, Plasma-catalytic removal of formaldehyde over Cu–Ce catalysts in a dielectric barrier discharge reactor, *Appl. Catal. B* 170–171 (2015) 293–300, <https://doi.org/10.1016/j.apcatb.2015.01.032>.
- [9] J. Quiroz Torres, S. Royer, J.P. Bellat, J.M. Giraudon, J.F. Lamonier, Formaldehyde: Catalytic oxidation as a promising soft way of elimination, *ChemSusChem* 6 (2013) 578–592, <https://doi.org/10.1002/cssc.201200809>.
- [10] D. Zhu, Y. Huang, J. Cao, S. Lee, M. Chen, Z. Shen, Cobalt nanoparticles encapsulated in porous nitrogen-doped carbon: oxygen activation and efficient catalytic removal of formaldehyde at room temperature, *Appl. Catal. B* 258 (2019) 117981, <https://doi.org/10.1016/j.apcatb.2019.117981>.
- [11] J. Pei, J.S. Zhang, Critical review of catalytic oxidation and chemisorption methods for indoor formaldehyde removal, *HVACR Res.* 17 (2011) 476–503, <https://doi.org/10.1080/10789669.2011.587587>.
- [12] C. Zhang, H. He, Ki. Tanaka, Perfect catalytic oxidation of formaldehyde over a Pt/TiO₂ catalyst at room temperature, *Catal. Commun.* 6 (2005) 211–214, <https://doi.org/10.1016/j.catcom.2004.12.012>.
- [13] C. Zhang, H. He, Ki. Tanaka, Catalytic performance and mechanism of a Pt/TiO₂ catalyst for the oxidation of formaldehyde at room temperature, *Appl. Catal. B* 65 (2006) 37–43, <https://doi.org/10.1016/j.apcatb.2005.12.010>.
- [14] X. Tang, J. Chen, X. Huang, Y. Xu, W. Shen, Pt/MnO_x–CeO₂ catalysts for the complete oxidation of formaldehyde at ambient temperature, *Appl. Catal. B* 81 (2008) 115–121, <https://doi.org/10.1016/j.apcatb.2007.12.007>.

- [15] C. Zhang, F. Liu, Y. Zhai, H. Ariga, N. Yi, Y. Liu, K. Asakura, M. Flytzani-Stephanopoulos, H. He, Alkali-Metal-Promoted Pt/TiO₂ opens a more efficient pathway to formaldehyde oxidation at ambient temperatures, *Angew. Chem., Int. Ed.* 51 (2012) 9628–9632, <https://doi.org/10.1002/anie.201202034>.
- [16] L. Nie, A. Meng, J. Yu, M. Jaroniec, Hierarchically macro-mesoporous Pt/γ-Al₂O₃ composite microspheres for efficient formaldehyde oxidation at room temperature, *Sci. Res. J.* 3 (2013) 3215, <https://doi.org/10.1038/srep03215>.
- [17] L. Nie, J. Yu, X. Li, B. Cheng, G. Liu, M. Jaroniec, Enhanced performance of NaOH-modified Pt/TiO₂ toward room temperature selective oxidation of formaldehyde, *Environ. Sci. Technol.* 47 (2013) 2777–2783, <https://doi.org/10.1021/es3045949>.
- [18] H. Huang, D.Y.C. Leung, Complete oxidation of formaldehyde at room temperature using TiO₂ supported metallic Pd nanoparticles, *ACS Catal.* 1 (2011) 348–354, <https://doi.org/10.1021/cs200023p>.
- [19] S.J. Park, I. Bae, I.S. Nam, B.K. Cho, S.M. Jung, J.H. Lee, Oxidation of formaldehyde over Pd/beta catalyst, *Chem. Eng. J.* 195 (2012) 392–402, <https://doi.org/10.1016/j.cej.2012.04.028>.
- [20] H. Huang, X. Ye, H. Huang, L. Zhang, D.Y.C. Leung, Mechanistic study on formaldehyde removal over Pd/TiO₂ catalysts: oxygen transfer and role of water vapor, *Chem. Eng. J.* 230 (2013) 73–79, <https://doi.org/10.1016/j.cej.2013.06.035>.
- [21] C. Zhang, Y. Li, Y. Wang, H. He, Sodium-promoted Pd/TiO₂ for catalytic oxidation of formaldehyde at ambient temperature, *Environ. Sci. Technol.* 48 (2014) 5816–5822, <https://doi.org/10.1021/es4056627>.
- [22] Y. Li, C. Zhang, H. He, J. Zhang, M. Chen, Influence of alkali metals on Pd/TiO₂ catalysts for catalytic oxidation of formaldehyde at room temperature, *Catal. Sci. Technol.* 6 (2016) 2289–2295, <https://doi.org/10.1039/c5cy01521a>.
- [23] Y. Li, C. Zhang, J. Ma, M. Chen, H. Deng, H. He, High temperature reduction dramatically promotes Pd/TiO₂ catalyst for ambient formaldehyde oxidation, *Appl. Catal. B* 217 (2017) 560–569, <https://doi.org/10.1016/j.apcatb.2017.06.023>.
- [24] K. Li, J. Ji, H. Huang, M. He, Efficient activation of Pd/CeO₂ catalyst by non-thermal plasma for complete oxidation of indoor formaldehyde at room temperature, *Chemosphere* 246 (2020) 125762–125768, <https://doi.org/10.1016/j.chemosphere.2019.125762>.
- [25] X. Sun, J. Lin, H. Guan, L. Li, L. Sun, Y. Wang, S. Miao, Y. Su, X. Wang, Complete oxidation of formaldehyde over TiO₂ supported subnanometer Rh catalyst at ambient temperature, *Appl. Catal. B* 226 (2018) 575–584, <https://doi.org/10.1016/j.apcatb.2018.01.011>.
- [26] C. Zhang, H. He, A comparative study of TiO₂ supported noble metal catalysts for the oxidation of formaldehyde at room temperature, *Catal. Today* 126 (2007) 345–350, <https://doi.org/10.1016/j.cattod.2007.06.010>.
- [27] Y. Li, X. Chen, C. Wang, C. Zhang, H. He, Sodium enhances Ir/TiO₂ activity for catalytic oxidation of formaldehyde at ambient temperature, *ACS Catal.* 8 (2018) 11377–11385, <https://doi.org/10.1021/acscatal.8b03026>.
- [28] C. Ma, D. Wang, W. Xue, B. Dou, H. Wang, Z. Hao, Investigation of formaldehyde oxidation over Co₃O₄–CeO₂ and Au/Co₃O₄–CeO₂ catalysts at room temperature: effective removal and determination of reaction mechanism, *Environ. Sci. Technol.* 45 (2011) 3628–3634, <https://doi.org/10.1021/es104146v>.
- [29] B. Liu, Y. Liu, C. Li, W. Hu, P. Jing, Q. Wang, J. Zhang, Three-dimensionally ordered macroporous Au/CeO₂–Co₃O₄ catalysts with nanoporous walls for enhanced catalytic oxidation of formaldehyde, *Appl. Catal. B* 127 (2012) 47–58, <https://doi.org/10.1016/j.apcatb.2012.08.005>.
- [30] Z. Wang, W. Wang, L. Zhang, D. Jiang, Surface oxygen vacancies on Co₃O₄ mediated catalytic formaldehyde oxidation at room temperature, *Catal. Sci. Technol.* 6 (2016) 3845–3853, <https://doi.org/10.1039/c5cy01709b>.
- [31] X. Tang, Y. Li, X. Huang, Y. Xu, H. Zhu, J. Wang, W. Shen, MnO_x–CeO₂ mixed oxide catalysts for complete oxidation of formaldehyde: effect of preparation method and calcination temperature, *Appl. Catal. B* 62 (2006) 265–273, <https://doi.org/10.1016/j.apcatb.2005.08.004>.
- [32] Y. Huang, B. Long, M. Tang, Z. Rui, M.S. Balogun, Y. Tong, H. Ji, Bifunctional catalytic material: an ultrastable and high-performance surface defect CeO₂ nanosheets for formaldehyde thermal oxidation and photocatalytic oxidation, *Appl. Catal. B* 181 (2016) 779–787, <https://doi.org/10.1016/j.apcatb.2015.08.047>.
- [33] Z. Qu, Y. Sun, D. Chen, Y. Wang, Possible sites of copper located on hydroxyapatite structure and the identification of active sites for formaldehyde oxidation, *J. Mol. Catal. A Chem.* 393 (2014) 182–190, <https://doi.org/10.1016/j.molcata.2014.06.008>.
- [34] J. Zhang, Y. Li, L. Wang, C. Zhang, H. He, Catalytic oxidation of formaldehyde over manganese oxides with different crystal structures, *Catal. Sci. Technol.* 5 (2015) 2305–2313, <https://doi.org/10.1039/c4cy01461h>.
- [35] S. Rong, T. He, P. Zhang, Self-assembly of MnO₂ nanostructures into high purity three-dimensional framework for high efficiency formaldehyde mineralization, *Appl. Catal. B* (2019) 118375, <https://doi.org/10.1016/j.apcatb.2019.118375>.
- [36] J. Wang, J. Li, C. Jiang, P. Zhou, P. Zhang, J. Yu, The effect of manganese vacancy in birnessite-type MnO₂ on room-temperature oxidation of formaldehyde in air, *Appl. Catal. B* 204 (2017) 147–155, <https://doi.org/10.1016/j.apcatb.2016.11.036>.
- [37] R. Fang, Q. Feng, H. Huang, J. Ji, M. He, Y. Zhan, B. Liu, D.Y.C. Leung, Effect of K⁺ ions on efficient room-temperature degradation of formaldehyde over MnO₂ catalysts, *Catal. Today* 327 (2019) 154–160, <https://doi.org/10.1016/j.cattod.2018.05.019>.
- [38] R. Fang, H. Huang, J. Ji, M. He, Q. Feng, Y. Zhan, D.Y.C. Leung, Efficient MnO_x supported on coconut shell activated carbon for catalytic oxidation of indoor formaldehyde at room temperature, *Chem. Eng. J.* 334 (2018) 2050–2057, <https://doi.org/10.1016/j.cej.2017.11.176>.
- [39] L. Zhang, Y. Xie, Y. Jiang, Y. Li, C. Wang, S. Han, H. Luan, X. Meng, F. Xiao, Mn-promoted Ag supported on pure siliceous Beta zeolite (Ag/Beta-Si) for catalytic combustion of formaldehyde, *Appl. Catal. B* 268 (2020) 118461–118466, <https://doi.org/10.1016/j.apcatb.2019.118461>.
- [40] Z. Huang, X. Gu, Q. Cao, P. Hu, J. Hao, J. Li, X. Tang, Catalytically active single-atom sites fabricated from silver particles, *Angew. Chem., Int. Ed.* 51 (2012) 4198–4203, <https://doi.org/10.1002/anie.201109065>.
- [41] D. Chen, Z. Qu, S. Shen, X. Li, Y. Shi, Y. Wang, Q. Fu, J. Wu, Comparative studies of silver based catalysts supported on different supports for the oxidation of formaldehyde, *Catal. Today* 175 (2011) 338–345, <https://doi.org/10.1016/j.cattod.2011.03.059>.
- [42] Z. Qu, S. Shen, D. Chen, Y. Wang, Highly active Ag/SBA-15 catalyst using post-grafting method for formaldehyde oxidation, *J. Mol. Catal. A Chem.* 356 (2012) 171–177, <https://doi.org/10.1016/j.molcata.2012.01.013>.
- [43] B. Bai, J. Li, Positive Effects of K⁺ ions on three-dimensional mesoporous Ag/Co₃O₄ catalyst for HCHO oxidation, *ACS Catal.* 4 (2014) 2753–2762, <https://doi.org/10.1021/cs5006663>.
- [44] P. Hu, Z. Amghouz, Z. Huang, F. Xu, Y. Chen, X. Tang, Surface-confined atomic silver centers catalyzing formaldehyde oxidation, *Environ. Sci. Technol.* 49 (2015) 2384–2390, <https://doi.org/10.1021/es504570n>.
- [45] J. Zhang, Y. Li, Y. Zhang, M. Chen, L. Wang, C. Zhang, H. He, Effect of support on the activity of Ag-based catalysts for formaldehyde oxidation, *Sci. Res. J.* 5 (2015) 12950, <https://doi.org/10.1038/srep12950>.
- [46] B. Bai, Q. Qiao, H. Arandiyani, J. Li, J. Hao, Three-dimensional ordered mesoporous MnO₂-supported Ag nanoparticles for catalytic removal of formaldehyde, *Environ. Sci. Technol.* 50 (2016) 2635–2640, <https://doi.org/10.1021/acs.est.5b03342>.
- [47] D. Chen, Z. Qu, Y. Sun, K. Gao, Y. Wang, Identification of reaction intermediates and mechanism responsible for highly active HCHO oxidation on Ag/MCM-41 catalysts, *Appl. Catal. B* 142–143 (2013) 838–848, <https://doi.org/10.1016/j.apcatb.2013.06.025>.
- [48] X. Chen, M. Chen, G. He, F. Wang, G. Xu, Y. Li, C. Zhang, H. He, Specific role of potassium in promoting Ag/Al₂O₃ for catalytic oxidation of formaldehyde at low temperature, *J. Phys. Chem. C* 122 (2018) 27331–27339, <https://doi.org/10.1021/acs.jpcc.8b07160>.
- [49] L. Ma, D. Wang, J. Li, B. Bai, L. Fu, Y. Li, Ag/CeO₂ nanospheres: efficient catalysts for formaldehyde oxidation, *Appl. Catal. B* 148–149 (2014) 36–43, <https://doi.org/10.1016/j.apcatb.2013.10.039>.
- [50] R. Fang, M. He, H. Huang, Q. Feng, J. Ji, Y. Zhan, D.Y.C. Leung, W. Zhao, Effect of redox state of Ag on indoor formaldehyde degradation over Ag/TiO₂ catalyst at room temperature, *Chemosphere* 213 (2018) 235–243, <https://doi.org/10.1016/j.chemosphere.2018.09.019>.
- [51] G. Kresse, J. Furthmüller, Efficiency of ab-initio total energy calculations for metals and semiconductors using a plane-wave basis set, *Comp. Mater. Sci.* 6 (1996) 15–50, [https://doi.org/10.1016/0927-0256\(96\)00008-0](https://doi.org/10.1016/0927-0256(96)00008-0).
- [52] P.E. Blochl, Projector augmented-wave method, *Phys. Rev. B* 50 (1994) 17953–17979, <https://doi.org/10.1103/PhysRevB.50.17953>.
- [53] G. Kresse, D. Joubert, From ultrasoft pseudopotentials to the projector augmented-wave method, *Phys. Rev. B* 59 (1999) 1758–1775, <https://doi.org/10.1103/PhysRevB.59.1758>.
- [54] J.P. Perdew, K. Burke, M. Ernzerhof, Generalized gradient approximation made simple, *Phys. Rev. Lett.* 77 (1996) 3865–3868, <https://doi.org/10.1103/PhysRevLett.77.3865>.
- [55] T. Keckés, J. Raskó, J. Kiss, FTIR and mass spectrometric studies on the interaction of formaldehyde with TiO₂ supported Pt and Au catalysts, *Appl. Catal. A Gen.* 273 (2004) 55–62, <https://doi.org/10.1016/j.apcata.2004.06.012>.
- [56] Y. He, H. Ji, In-situ DRIFTS study on catalytic oxidation of formaldehyde over Pt/TiO₂ under mild conditions, *Chinese J. Catal.* 31 (2010) 171–175, <https://doi.org/10.3724/sp.j.1088.2010.90904>.
- [57] X. Chen, G. He, Y. Li, M. Chen, X. Qin, C. Zhang, H. He, Identification of a facile pathway for dioxymethylene conversion to formate catalyzed by surface hydroxyl on TiO₂-based catalyst, *ACS Catal.* 10 (2020) 9706–9715, <https://doi.org/10.1021/acscatal.0c01901>.
- [58] X. Tang, J. Chen, Y. Li, Y. Xu, W. Shen, Complete oxidation of formaldehyde over Ag/MnO_x–CeO₂ catalysts, *Chem. Eng. J.* 118 (2006) 119–125, <https://doi.org/10.1016/j.cej.2006.02.002>.
- [59] F. Wang, J. Ma, G. He, M. Chen, C. Zhang, H. He, Nanosize effect of Al₂O₃ in Ag/Al₂O₃ catalyst for the selective catalytic oxidation of ammonia, *ACS Catal.* 8 (2018) 2670–2682, <https://doi.org/10.1021/acscatal.7b03799>.
- [60] X. Wang, X. Han, Y. Huang, J. Sun, S. Xu, X. Bao, ¹⁷O solid-state NMR study on the size dependence of oxygen activation over silver catalysts, *J. Phys. Chem. C* 116 (2012) 25846–25851, <https://doi.org/10.1021/jp308637z>.
- [61] M. Lamoth, M. Plodinec, L. Scharfenberg, S. Wrabetz, F. Girgsdies, T. Jones, F. Rosowski, R. Horn, R. Schlögl, E. Frei, Supported Ag nanoparticles and clusters for CO oxidation: size effects and influence of the silver–oxygen interactions, *ACS Appl. Nano Mater.* 2 (2019) 2909–2920, <https://doi.org/10.1021/acsnm.9b00344>.